Evolving into a remnant: optical observations of SN 1978K at three decades

H. Kuncarayakti,[1,2]★ K. Maeda,[3,4]★ J. P. Anderson,[5] M. Hamuy,[1,2] K. Nomoto,[4]† L. Galbany[1,2] and M. Doi[6,7]

[1]*Millennium Institute of Astrophysics (MAS), Casilla 36-D, Santiago, Chile*
[2]*Departamento de Astronomía, Universidad de Chile, Casilla 36-D, Santiago, Chile*
[3]*Department of Astronomy, Kyoto University, Kitashirakawa-Oiwake-cho, Sakyo-ku, Kyoto 606-8502, Japan*
[4]*Kavli Institute for the Physics and Mathematics of the Universe (WPI), University of Tokyo, Kashiwa, Chiba 277-8583, Japan*
[5]*European Southern Observatory, Alonso de Córdova 3107, Vitacura, Santiago, Chile*
[6]*Institute of Astronomy, Graduate School of Science, The University of Tokyo, 2-21-1 Osawa, Mitaka, Tokyo 181-0015, Japan*
[7]*Research Center for the Early Universe, Graduate School of Science, The University of Tokyo, Bunkyo-ku, Tokyo 113-003, Japan*

ABSTRACT

We present new optical observations of the supernova SN 1978K, obtained in 2007 and 2014 with the Very Large Telescope. We discover that the supernova has not faded significantly, even more than three decades after its explosion. The spectrum exhibits numerous narrow (FWHM $\lesssim 600\,\mathrm{km\,s^{-1}}$) emission lines, indicating that the supernova blastwave is persistently interacting with dense circumstellar material (CSM). Evolution of emission lines indicates that the supernova ejecta is slowly progressing through the reverse shock, and has not expanded past the outer edge of the circumstellar envelope. We demonstrate that the CSM is not likely to be spherically distributed, with mass of $\lesssim 1\,\mathrm{M_\odot}$. The progenitor mass loss rate is estimated as $\gtrsim 0.01\,\mathrm{M_\odot\,yr^{-1}}$. The slowly fading late-time light curve and spectra show striking similarity with SN 1987A, indicating that a rate at which the CSM is being swept-up by the blastwave is gradually decaying and SN 1978K is undergoing similar evolution to become a remnant. Due to its proximity (4 Mpc), SN 1978K serves as the next best example of late-time supernova evolution after SN 1987A.

Key words: supernovae: general – supernovae: individual: SN 1978K.

1 INTRODUCTION

SN 1978K was first discovered in 1990 as a strong Hα source during a survey of H II regions in the nearby spiral galaxy NGC 1313 (Dopita & Ryder 1990). The object was initially classified as a nova, with a nebular spectrum exhibiting strong emission lines, until further observations suggested that it was actually a supernova (SN) well into the late-time phase (Ryder et al. 1993). The SN still radiates strongly in X-ray and radio wavelengths for many years after the supposed explosion in mid-1978, indicating an on-going interaction of the SN ejecta with dense circumstellar medium(CSM; Ryder et al. 1993; Chugai, Danziger & della Valle 1995; Chu et al. 1999; Schlegel et al. 1999; Gruendl et al. 2002; Lenz & Schlegel 2007; Smith et al. 2007).

Ryder et al. (1993) reported that a possible progenitor of SN 1978K has been identified in pre-explosion photographic plates, having $B_J = 22.1$ mag, in 1974–1975. With their adopted distance to NGC 1313 of 4.5 Mpc ($\mu = 28.3$ mag) and assuming no reddening, that magnitude would correspond to a luminous blue object with absolute magnitude of ~ -6 mag. The object seemed to fade below $B_J \sim 23$ in 1977 Oct, then came into outburst in 1978. Only four data points in the light curve were recovered from the 1978 outburst, with brightest magnitude $B = 16.0$ reached on 1978 Jul 31, and no spectroscopic data exist during the early phase. Therefore, the actual SN-type classification of this object is unknown although late-time observations show that the CSM is hydrogen-rich, suggesting a Type-II event.

Chu et al. (1999) suggested that SN 1978K is associated with CSM similar to the ejecta nebulae of luminous blue variable (LBV) stars, based on the detection of the narrow components of Hα and [N II] in high-resolution spectroscopy, which were interpreted as having originated in the unshocked CSM. This detection was also later confirmed by Gruendl et al. (2002). LBV stars such as η Car and P Cyg are evolved massive stars that have been known to undergo irregular variability and eruptive mass loss episodes. A good number of SNe IIn have been associated with LBV progenitors (see e.g. Gal-Yam & Leonard 2009; Smith et al. 2011; Kiewe et al.

★E-mail: kuncarayakti@gmail.com (HK); keiichi.maeda@kusastro.kyoto-u.ac.jp (KM)
†Hamamatsu Professor

2012; Taddia et al. 2013). While the connection between LBV stars and Type-IIn SNe has often been suggested in the recent literature, alternatively red supergiant stars have also been proposed as one viable progenitor for this kind of objects (e.g. SN 1998S; Mauerhan & Smith 2012).

SN 1978K is arguably unique among other SNe observed at very late times. The emission lines are evidently narrow (full width at half-maximum; FWHM $\sim$few hundred km s^{-1}) and long-lasting, with a wealth of various species in addition to the commonly detected Hα, Hβ, and oxygen lines. For comparison, SNe 1986J and 1979C observed at the age of $\sim$20 yr only show a few such lines (Milisavljevic et al. 2008, 2009), which was also the case for SNe 1957D, 1970G, 1980K, and 1993J (Milisavljevic et al. 2012). Those SNe observed at late times typically show FWHM velocities in the order of several thousands km s^{-1}, significantly higher than that of SN 1978K. SN 1986J, for example, exhibits spectra containing dominant Hα emission with unchanging width between 1986 and 1989 ($\sim$4–7 yr after the supposed explosion time, Leibundgut et al. 1991), and later observations in 1991 and 2007 show that the width had not changed significantly (Milisavljevic et al. 2008) although the line luminosity diminished greatly during that time period.

Optical spectra of SN 1978K were previously obtained in 1990 (Ryder et al. 1993, henceforth R93), 1992 (Chugai et al. 1995, henceforth C95), 1996 (Schlegel et al. 1999, henceforth S99), 1997 (Chu et al. 1999), and 2000 (Gruendl et al. 2002). The 1990–1996 spectra were obtained in low resolution ($\sim$10 Å) while the 1997/2000 ones were in high-resolution echelle spectroscopy ($\sim$0.3 Å). Here, we report the spectroscopy of SN 1978K conducted in 2014 i.e. more than a decade after the last published spectrum and 36 yr after the SN explosion, as well as archival spectra and photometry taken in 2007, and discuss the physical properties of the object derived from the observational data. The paper proceeds with Section 2 describing the observations and data reduction, Section 3 with the results then Section 4 with the discussions, and ends with the summary.

2 OBSERVATIONS AND DATA REDUCTION

SN 1978K was observed using the UT3/Melipal unit of the Very Large Telescope (VLT) at Cerro Paranal Observatory, Chile, and the VIMOS instrument in integral field unit (IFU) mode (Le Fèvre et al. 2003). The observation was done as part of an IFU survey[1] of nearby SN explosion sites to study the underlying stellar populations (Kuncarayakti et al. 2015). Sky conditions during the observation on 2014 November 25 (UT) were photometric, with seeing varying between 0.5 arcsec and 0.8 arcsec during the 2 × 1800 s exposure of the object. The final image quality measured on the reduced data cube is around 1 arcsec.

VIMOS was used in the IFU medium resolution mode with 13 arcsec × 13 arcsec field of view at the scale of 0.33 arcsec per spaxel. The spectral coverage is 4800–10 000 Å, with dispersion of 2.6 Å pixel^{-1}. The effective line FWHM of the spectrum is $\approx$8 Å. Spectrophotometric standard stars were also observed during the same night for the purpose of absolute flux calibration. The raw data were reduced using the REFLEX[2]-based VIMOS IFU pipeline (Freudling et al. 2013), resulting in two wavelength- and flux-calibrated data cubes in (x, y, λ) format for each of the 1800 s

exposures. The two data cubes were averaged and then the resulting final data cube was analysed using QFITSVIEW[3] (Ott 2012).

SN 1978K was identified in the IFU field of view and then the spectrum was extracted from the final science data cube using apertures with radius of 2 and 4 spaxels, corresponding to 0.66 arcsec and 1.32 arcsec, respectively. These apertures were chosen as the radial profile of the SN is not perfectly Gaussian, with range in FWHM around 2–4 spaxels. This is most likely an artefact of the observation and data reduction. The sky background was estimated and removed by using an annulus surrounding the extraction aperture. The spectrum resulting from 4 spaxels aperture radius is more noisy compared to that from 2 spaxels radius due to increased sky contamination. On the other hand, the 2 spaxels spectrum does not contain the whole flux from the object since the aperture misses the outer wings of the point spread function. Therefore, we scaled the flux of the 2 spaxels spectrum to match the flux of the 4 spaxels one, with Hα line flux as a reference. This scaled spectrum is used in the subsequent spectral analysis using the ONEDSPEC package in IRAF.[4] Synthetic *VRI* magnitudes were calculated from the spectrum, resulting in $V_{synth} = 20.7$, $R_{synth} = 19.3$, and $I_{synth} = 19.8$ with estimated errors of $\approx$0.2 mag.

Additionally, we found and recovered raw photometric and spectroscopic data of SN 1978K in the European Southern Observatory (ESO) Science Archive Facility,[5] taken from VLT/FORS2 (Appenzeller et al. 1998) observations in 2007.[6] The data were obtained in two different nights of observation: 2007 July 25 (photometry, *BVRI* bands and spectroscopy, *RIz* bands) and 2007 September 26 (spectroscopy, *B* band) under clear sky conditions. Seeing varied between 0.9 arcsec and 1.4 arcsec (photometry) and 0.6 arcsec and 0.8 arcsec (spectroscopy). The spectroscopy uses the 1 arcsec longslit with the GRIS_600B, GRIS_600RI, and GRIS_600z grism configurations. Exposure times were (2, 4, 4) × 900 s for each grism, respectively. This resulted in three spectra covering three wavelength regions (3500–6000 Å, 5300–8500 Å, 7500–10 500 Å) with dispersion of 0.8 Å pixel^{-1}. After raw data reduction using the REFLEX-based FORS2 pipeline, both the spectroscopic and photometric data were flux calibrated using spectrophotometric and photometric standard star observations (Landolt 2009). The three spectra were later combined together by averaging overlapping wavelength regions and analysed using IRAF as with the 2014 spectrum. Photometry was achieved using the APPHOT aperture photometry package within IRAF. The synthetic *B* and *I* magnitudes calculated from the spectrum agree with magnitudes resulting from direct imaging within 0.1 mag. The *R*-band image however, was not usable as SN 1978K was saturated. Therefore, we use the synthetic *R*-band magnitude for the subsequent analyses. The 2007 magnitudes are $B = 20.6$, $V = 20.4$, $R_{synth} = 19.2$, $I = 20.1$.

Throughout the paper we adopt the distance to NGC 1313 as 4.61 ± 0.21 pc ($\mu = 28.3$ mag), according to the new Cepheid distance measurement using *Hubble Space Telescope* by Qing et al. (2015). This is slightly different compared to the value of 4.5 Mpc used in R93, C95, and S99, and 4.13 Mpc in Smith et al. (2007) and Lenz & Schlegel (2007).

---

[1] ESO observing programme 094.D-0290 (PI: Kuncarayakti).

[2] https://www.eso.org/sci/software/reflex/
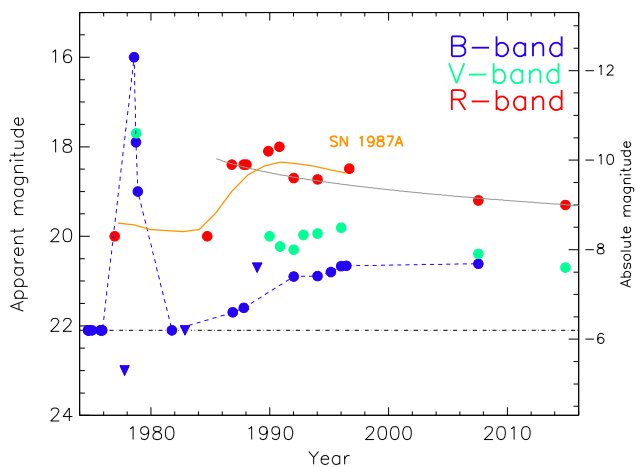
[3] http://www.mpe.mpg.de/~ott/dpuser/qfitsview.html

[4] IRAF is distributed by the National Optical Astronomy Observatory, which is operated by the Association of Universities for Research in Astronomy (AURA) under cooperative agreement with the National Science Foundation.

[5] http://archive.eso.org/eso/eso_archive_main.html

[6] ESO observing programme 079.D-0124 (PI: Kjaer).

Figure 1. Light curve of SN 1978K between 1974 and 2014. The absolute magnitude axis assumes no reddening. The horizontal dash–dotted line indicates the apparent magnitude of the progenitor star. *B*-band magnitudes are connected with dashed lines for clarity. Inverted triangles denote upper limits. Typical error in photometry is 0.3 mag. The solid orange line represents an approximation to SN 1987A *R*-band light curve after the interaction with the CSM ring (Fransson et al. 2015), unscaled but shifted to match SN 1978K epoch and magnitudes. The grey solid line indicates power-law decay of the CSM interaction in SN 1978K (see text).

3 RESULTS

3.1 Light curve

In Fig. 1 the historic light curve of SN 1978K is presented. Photometric data points from R93 and S99 are plotted alongside our 2007/2014 photometry. As has been reported by R93, the light-curve evolution during the actual outburst event in 1978 was not well covered. Therefore, the peak in the light curve does not correspond to the actual event of maximum brightness of SN 1978K. Shortly prior to the 1978 eruption, the progenitor curiously became fainter in blue. While no information on the redder bands exist, it is possible that it expanded to become cooler and redder.

Looking at the post-1978 light curve, it seems that there is a significant increase in brightness starting around mid-1980s. The *R* magnitude brightened from 20.0 in 1984 September, to 18.4 in 1986 October. The *V* and *B* bands also seem to follow this behaviour. After the sudden increase, the luminosity went down gradually until our latest observation in 2014. This sudden increase is interpreted as the onset of the interaction between the SN blastwave and the surrounding CSM, analogous to what was experienced by SN 1987A. We discuss this interaction and comparison to SN 1987A in Section 4, where the two SNe show analogous late-time light curves and spectra.

3.2 Optical spectrum

The FORS2 and VIMOS spectra of SN 1978K at year 2007 and 2014 are shown in Fig. 2, together with a synthetic spectrum representing the one taken in 1992 (C95) for comparison. The original 1992 EFOSC2 raw data were not available for retrieval in the ESO archives. Therefore, the 1992 spectrum was generated by constructing Gaussian curves with FWHM of $560\,\mathrm{km\,s^{-1}}$, the observed Hα FWHM which is comparable to the instrumental FWHM of the 1992 spectrum, and using tabulated wavelength and line fluxes in C95 to position the lines along the wavelength axis and scale the line strengths.

Overall, the spectra show very similar appearances, which indicates that the same physical process is still continuing after two decades. The spectra are dominated by narrow emission lines, in particular Hα is the strongest, and also numerous other lines from various elements primarily helium, oxygen, and iron. The spectra of R93 and S99 also show a similar appearance with the spectra displayed here in Fig. 2, although of a somewhat lower signal-to-noise ratio.

We measure the line fluxes in the 2007/2014 spectra by fitting Gaussian profiles to the lines, after removing the very weak continuum component by fitting a linear function. We also applied deblending process in case two nearby lines are not well separated. Table 1 lists the lines identified in the spectrum. Line identifications follow that of SN 1987A (Gröningsson et al. 2008) and SN 2009kn (Kankare et al. 2012). We identified most of the lines within our spectral wavelength range originally detected in 1992, with the exception of the ambiguous [Fe x] coronal line. [Fe x] $\lambda6374$ is possibly blended with the much stronger [O I] $\lambda6364$ line. Another coronal line, [Fe XIV] $\lambda5303$ is clearly detected, although blended with the nearby [Fe II] $\lambda5297$. However, the two lines are of comparable strengths, and therefore could be more easily deblended compared to the [Fe x]–[O I] blending. These two coronal lines are indicative of a hot ($\sim10^6$ K) shocked gas (C95).

In the 2007/2014 spectra we also detected other lines redward of ~7000 Å, which were not detected or beyond the instrument response in the spectra taken in the 1990s. Redward of He I $\lambda7065$, we detected [Fe II] $\lambda7155$, and also a complex of lines around 7200–7400 Å. Among these lines, the [Ca II] doublet of $\lambda\lambda7291$, 7324 was detected, with possible contamination from He I $\lambda7281$ and [O II] λ 7330. [Ni II] lines at 7378, 7412 Å are present. We also detect [Cr II] lines at 8000, 8125, 8230 Å. Further away we detected a strong line at a rest wavelength of 8617 Å, possibly Fe II λ 8620, another unidentified line at $\lambda_0 = 9177$ Å, and a line at $\lambda_0 = 9227$ Å. The latter could be a blend of Pa9 $\lambda9229$ and [Fe II]$\lambda9227$ (see e.g. Gröningsson et al. 2008), or Mg II $\lambda\lambda9218$, 9244 (Fransson et al. 2013). [S III] $\lambda9531$ is detected, very close to Pa8 $\lambda9546$. In the 2007 spectrum we also detected Paδ $\lambda10049$ and unidentified infrared lines around 10285, 10317, 10332 Å, and a prominent line at 10399 Å with strength comparable to He I $\lambda5876$.

Other lines of particular interest are those at observed wavelength ~5537 Å, and [O I] $\lambda5577$ whose presence was reported by R93 but not by C95 and S99. This [O I] $\lambda5577$ is most probably a night sky emission[7] which was not clearly subtracted. This subtraction residual is also present in our spectra and the 1992 spectrum in C95. Blueward of this line, the intriguing line at 5537 Å was also clearly visible in the 1992 spectrum, but somehow not reported in the C95 paper. The line is not seen in the 1990 and 1996 spectra. Correcting from Doppler shift of $471\,\mathrm{km\,s^{-1}}$ as measured from the Hα line, the rest-frame wavelength of this line would be 5529 Å. This line is probably the [Fe II] $\lambda5528$ line as seen in SN 1987A spectrum and reported in Gröningsson et al. (2008).

3.3 Evolution of spectral line strengths

We first examine the evolution of the Hα flux as the strongest line in the optical regime. The observed Hα flux in 2014 (2007) is 4.4 (4.5) $\times 10^{-14}$ erg cm^{-2} s^{-1}, corresponding to the luminosity of 1.12 (1.14) $\times 10^{38}$ erg s^{-1}. As with the 1992 spectrum where the

---

[7] R93 mentioned in their table 3 that this line is blended with [O I] night sky line.
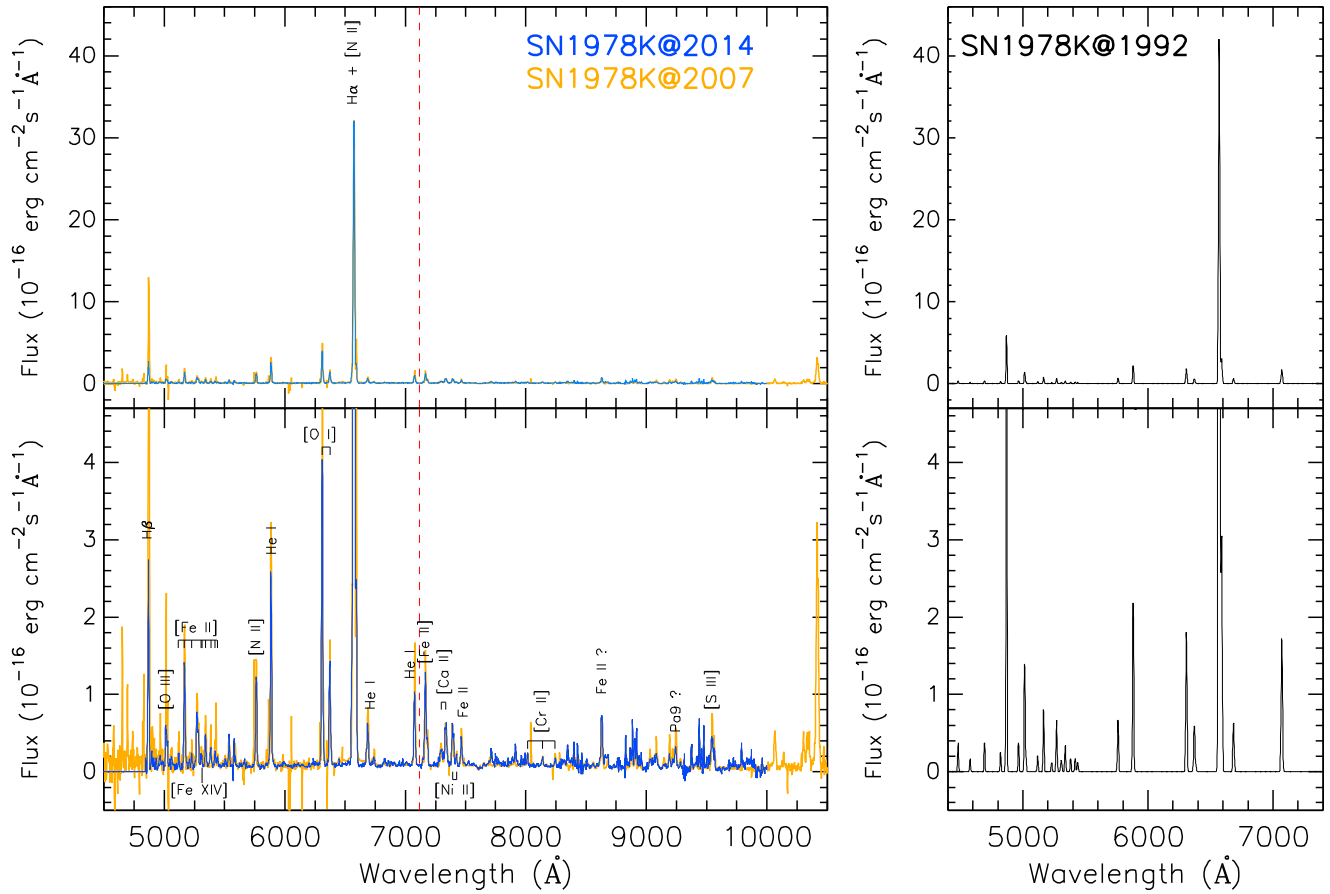
Figure 2. Observed spectra of SN 1978K in 2014 November and 2007 July (left-hand panels), compared to the 1992 spectrum (right-hand panels). Both left-hand and right-hand panels share the same scale in the plots. Upper panels shows the full coverage of the flux axis while bottom panels show the zoom-in to better examine the weaker lines. Spectra are not reddening-corrected. The red vertical dashed line indicates the red wavelength cutoff of the 1992 spectrum.

line identifications are near-complete, Hα contributes to roughly 60 per cent of the total line luminosity in the optical. Fig. 3 shows the evolution of Hα luminosity from 1990 to 2014 using also the spectra from R93, C95, and S99. We dereddened the flux from a total line-of-sight absorption of $A_B = 2$ mag (R93), assuming $R_V = 3.1$ and interstellar extinction law of Cardelli, Clayton & Mathis (1989). We note that this corresponds to $A_V = 1.5$ mag, while C95 quoted $A_V = 0.64$ from the same R93 source. The unreddened Hα luminosity in 2014 (2007) is thus 3.47 (3.55) $\times 10^{38}$ erg s^{-1}.

From Fig. 3 it is evident that the Hα luminosity has been decreasing slowly since 1992. As reported by C95, the Hα luminosity peaked around 1990, from which point afterwards it decreases. Also in Fig. 2 it is evident that the Hα line in 2014 is weaker compared to 1992, although not significantly. Chevalier & Fransson (1994) modelled late-time emission from Type-II SNe interacting with circumstellar material. It was predicted that as the reverse shock weakens with time, the Hα luminosity would also decrease steadily. We plot this prediction (table 6 of Chevalier & Fransson 1994) in Fig. 3 as the blue solid line, after scaling up by two orders of magnitude and taking 1978.0 as the time of the explosion. The slowly decreasing behaviour of data points between 1990 and 2014 resembles that of the model, although the sharp drop from 1990 to 1992 does not.

To examine the evolution of other lines, we plot the line ratios with respect to Hα from 1990 to 2014 in Fig. 4. In this plot, a systematic decrease in line ratio with time would result in a red–orange–green–blue–purple vertical sequence, and the opposite for

an increase. From the plot, it is evident that the lines exhibit various behaviours.
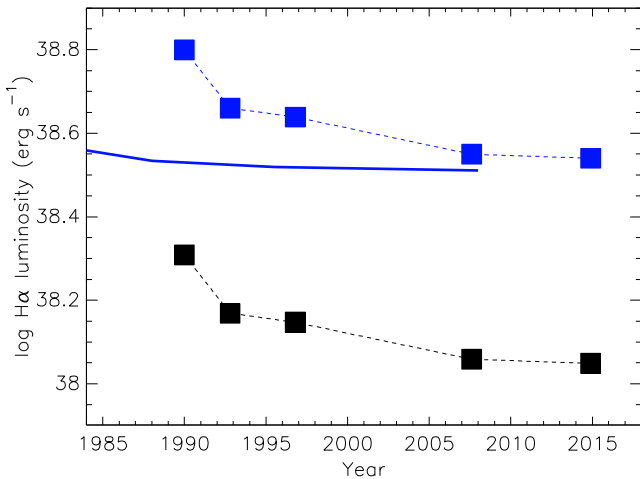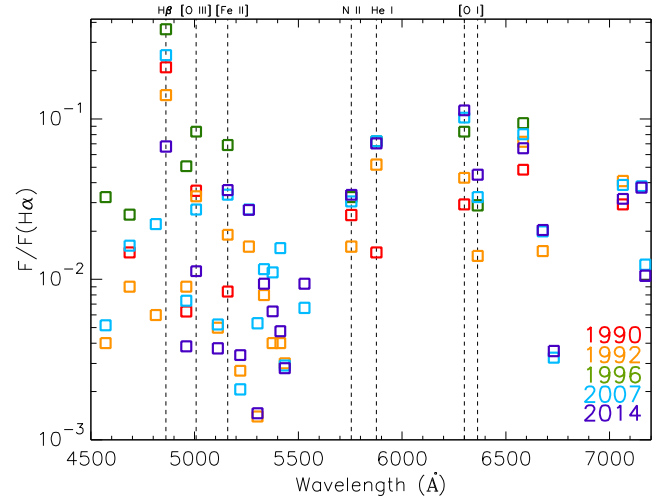
The Hβ/Hα ratio, or the inverse Balmer decrement, decreases from 1990 to 1992, but shoots up in 1996, decreases in 2007 and then drops again in 2014. The same behaviour is also seen in the [O III] line. It is to be noted that the spectra obtained in the 1990s were taken with slit spectroscopy that may have been affected by slit-loss and differential atmospheric refraction effects, which did not affect the 2014 spectrum taken with IFU spectroscopy. FORS2, while working in slit spectrosocpy mode, is equipped with an Atmospheric Dispersion Corrector. S99 mentioned that their 1996 spectrum may have suffered from differential refraction, causing them to lose more of the red light compared to the blue. This may explain the behaviour seen in the ratio of lines bluer than 5500 Å, where all the 1996 data points are higher up compared to the others. In the red part of the spectrum where the differential refraction effect is weaker the systematic behaviour is more visible. The [O I] doublet shows a systematic increase from 1990 to 2014. Comparing the 1992 and 2007/2014 spectra, it is apparent that generally the Hα line becomes weaker relative to the helium, oxygen, and iron lines.

3.4 SN 1978k environment

SN 1978K exploded in the south-western outskirts of NGC 1313, a barred spiral galaxy. NGC 1313 is actively star forming, and has been suspected to suffer interaction with a tidally disrupted

Table 1. Observed line strengths relative to $F(H\alpha) = 1000$.

Ion	λ_0 [Å]	$F/F(H\alpha)$ 2007	$F/F(H\alpha)$ 2014
Hβ	4861.3	250.2	67.3
[O III]	4958.9	7.4	3.8
[O III]	5006.8	27.2	11.3
He I	5015.7	9.3	6.7
[Fe II]	5111.6	5.2	3.7
[Fe II]	5158.8	33.8	36.0
[Fe II]	5220.1	2.1	3.4
[Fe II]	5261.6	27.2	27.1
[Fe XIV]	5302.9	5.3	1.5
[Fe II]	5333.6	11.6	9.4
[Fe II]	5376.5	11.1	6.3
[Fe II]	5413.0	15.7	4.7
[Fe II]	5433.1	2.9	2.8
[Fe II]	5527.6	6.6	9.4
[N II]	5754.5	30.6	33.6
He I	5875.7	72.6	70.5
[O I]	6300.3	101.8	113.0
[O I]	6363.8	32.7	44.9
Hα	6562.8	1000.0	1000.0
[N II]	6583.3	80.3	65.7
He I	6678.2	19.9	20.3
[S II]	6716.4	1.1	0.7
[S II]	6730.8	3.3	3.6
He I	7065.7	38.8	31.8
[Fe I]	7155.2	38.2	37.3
[Fe II]	7172.0	12.3	10.6
[Ca II] (+ He I)	7291.5	9.4	12.9
[Ca II] (+ [O II])	7323.9	24.9	25.9
[Ni II] (+ [Fe II])	7377.8	22.7	23.8
[Ni II]	7411.6	4.8	4.6
[Fe II]	7452.5	11.9	12.2
[Cr II]	8000.1	4.1	4.2
[Cr II]	8125.3	3.0	3.4
[Cr II]	8229.7	4.1	2.6
Fe II?	8617	16.6	24.7
?	9177	12.1	4.3
Pa9 + [Fe II] or Mg II	9227	17.8	8.7
[S III]	9530.6	18.03	19.2

Figure 4. Evolution of line fluxes compared to Hα, from 1990 to 2014. Prominent lines are identified with vertical dashed lines. The weak He I $\lambda5016$ line is not plotted for clarity, due to its proximity to [O III] $\lambda5007$.
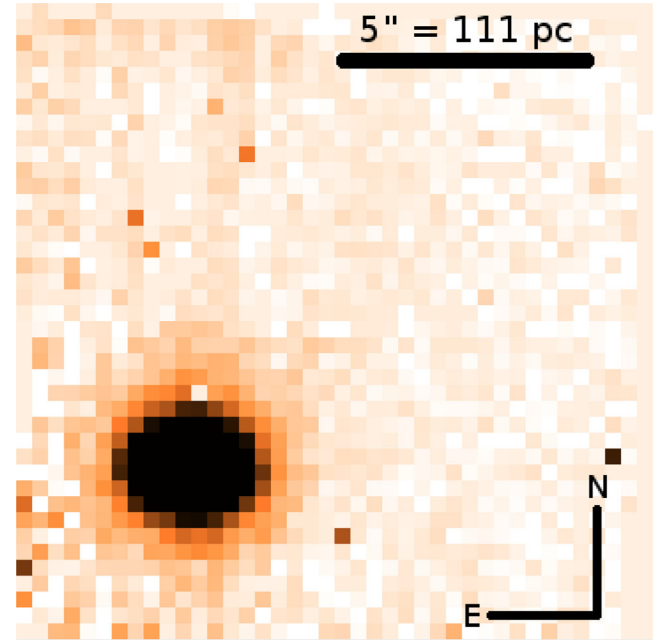
Figure 5. IFU field of view of SN 1978K in continuum-subtracted Hα emission. The SN is the only visible source in the field.

Figure 3. Hα line luminosity evolution, 1990–2014. Black and blue data points show observed and dereddened flux, respectively. Blue solid curve denotes the prediction of Hα luminosity evolution from the Type II SN model of Chevalier & Fransson (1994), shifted upward by two orders of magnitude.

satellite galaxy (see e.g. Silva-Villa & Larsen 2012, and references therein). H I observations also show the presence of an expanding superbubble which is likely to have originated from this interaction (Ryder et al. 1995). The star formation rate is elevated in the south-eastern region of NGC 1313 and the star formation history suggests a recent, local starburst as opposed to a global starburst affecting the whole galaxy. SN 1978K lies within this south-western interaction region, thus it is quite likely that its progenitor was associated with the starburst.

Our IFU data however, does not show any appreciable star formation within $\sim$50 pc from SN 1978K and several hundred pc in the north and west directions (Fig. 5). In any wavelength bin, whether in emission lines or continuum, the SN is the only source visible in the field. We do not detect any Hα emission down to $\sim$10^{-17} erg cm^{-2} s^{-1} Å^{-1}, corresponding to Hα luminosity of $\sim$10^{35} erg s^{-1}.
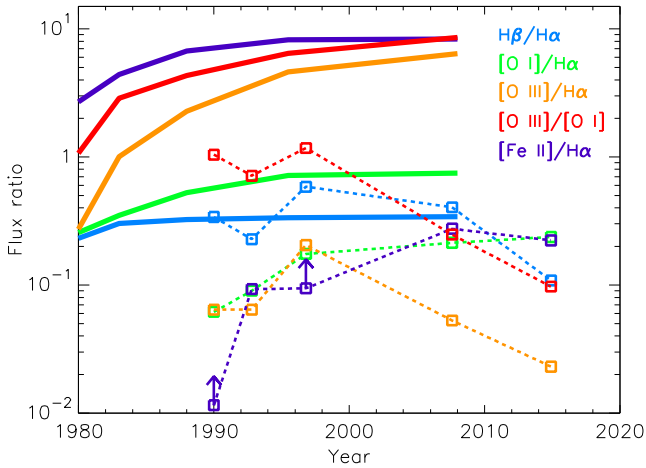
Figure 6. Line ratio evolution compared to the model by Chevalier & Fransson (1994). The model is represented with solid lines, while the observed data points with squares. Arrows indicate lower limits for the [Fe II] lines as the weaker lines were not detected in 1990 and 1996 spectra (see text for details).

This implies that even a small H II region similar to the Orion nebula ($L_{H\alpha} \approx 10^{37}$ erg s^{-1}; Crowther 2013) would have been well detected in our IFU data.

4 DISCUSSIONS

4.1 Spectral evolution and the CSM

C95 provided an explanation of the observed spectrum of SN 1978K as originating from radiative shock waves resulting from the interaction between the SN ejecta and dense clouds of circumstellar wind. In this picture the SN ejecta ploughs through the CSM, generating a reverse shock that is followed by a hot cooling region that is responsible for the Hα emission and then the cool, partially ionized ejecta. This partially ionized region is responsible for the emission of low-ionization lines such as [Fe II] and [O I] lines. As time passes, this outflowing, more metal-rich region of SN ejecta would overtake the reverse shock region and as a result the [Fe II] and [O I] line luminosities would increase compared to Hα. This is exactly what is observed, as shown in Fig. 6. The model of emission from CSM interaction in Type-II SNe by Chevalier & Fransson (1994) includes the evolution of line strengths. However, their model does not predict the same line ratio as observed (Fig. 6). This discrepancy has also been reported by Mauerhan & Smith (2012) who followed the evolution of SN 1998S at 14 yr, and suggested that it probably stems from the uncertainty in the model to the shock velocity and ejecta density. Below we further discuss the discrepancy between the observed behaviours in SN 1978K and Chevalier & Fransson (1994)'s model.

Fig. 6 shows the evolution of line ratios Hβ/Hα, [O I]/Hα, [O III]/Hα, [O III]/[O I], and [Fe II]/Hα. Here the [O I] flux is the combined flux of the doublet at $\lambda\lambda$6300, 6364, the [O III] combines $\lambda\lambda$4959, 5007, and [Fe II] combines all the flux of the [Fe II] lines. Upward arrows in the figure denote lower limits since in the 1990 and 1996 spectra only the [Fe II] λ5159 line was detected among the [Fe II] lines. The ratio Hβ/Hα is predicted to be increasing with time. The observed ratios closely match the predicted amount of the ratio although the behaviour is reversed, i.e. Hβ/Hα is observed to be generally decreasing. For the other lines, the amounts predicted by the models deviate significantly from the observations. Also the
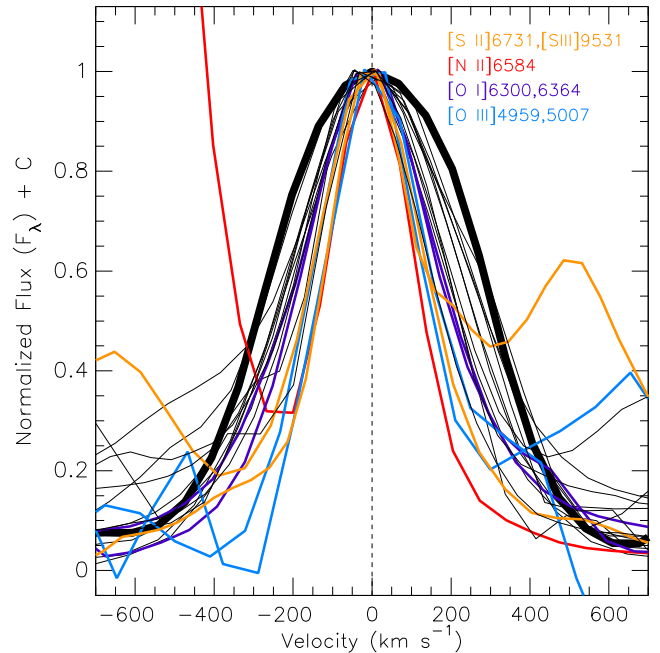
Figure 7. Velocity profiles of the strongest emission lines in the 2007 spectrum that are not contaminated by a neighbouring line. Hα is indicated with bold line and the narrowest lines are coloured.

line ratios are expected to be increasing with time, a behaviour that is only observed in [O I]/Hα and [Fe II]/Hα. The decreasing line ratios of the bluer lines with respect to Hα could have been caused by dust formation, which cause them to suffer greater reddening compared to Hα. However, from the line profiles alone there is no obvious evidence for the presence of dust.

The model by Chevalier & Fransson (1994) assumes a CSM that was created by wind with smoothly decreasing density, inversely proportional to the radius squared, r^{-2}. In this model, the Balmer and the low-ionization lines are both associated with the cooling shell which is created by the interaction suffering a rapid cooling. The high-ionization lines are emitted by the unshocked ejecta that are ionized by the high-energy radiation from the interacting region. With a density decrease in the cooling shell, the Balmer decrement (Hα/Hβ) also decreases as Hα becomes progressively optically thin. At the same time, it leads to the increasing importance of the forbidden lines. In this case, similar behaviour would be displayed by *both* the Balmer lines and the low-ionization (i.e. [O I], [Fe II]) lines, either together they behave in accordance to the model prediction or opposite to it. The fact that the two lines show different behaviours suggests that there are different regions of emission for these lines and the CSM cannot be approximated with a simple spherically symmetric distribution. Furthermore, this is supported by the observed decrease of the inverse Balmer decrement, Hβ/Hα ratio, which requires a density increase in the emitting region, or else an increase in the reddening.

In Fig. 7, we plot the strongest lines in our 2007 spectrum in velocity space. It is clearly seen that most of the lines closely follow a symmetric, Gaussian-like profile with average FWHM of 500 ± 100 km s^{-1}. The narrowest lines are [O III], [S II], and [N II] forbidden lines. They exhibit velocity FWHM of 300–400 km s^{-1}, in contrast with the 580 km s^{-1} velocity seen in Hα. These lines are commonly seen in normal H II regions, thus it is likely that they originate in the unshocked CSM further outside from the interaction region unlike what is assumed in the Chevalier & Fransson (1994) model.

Smith et al. ([2007](#)) reported the very long baseline interferometry (VLBI) detection of the remnant of SN 1978K. This remnant was marginally resolved and extends to ~10 mas, corresponding to a diameter of 0.2 pc. If the ejecta are assumed to be expanding constantly at 500 km s^{-1} since the time of the explosion as derived from the line FWHM, it would reach ~0.03 pc size. However, the observed size is considerably larger thus it is more likely that the unimpeded SN ejecta expands with velocity in the order of several thousand km s^{-1} as typically seen in other SNe. Bartel et al. ([2007](#)) showed that the outer boundary of radio emission is associated with the forward shock in a SN ejecta. The ~500 km s^{-1} velocity seen in the emission lines corresponds to the expansion velocity of the emitting regions. The narrow Hα and [N II] lines observed by Chu et al. ([1999](#)) using echelle spectroscopy show velocities of the order of 70–100 km s^{-1}, which is the velocity of the dense wind constituting the unshocked CSM. The data presented here do not have such high resolution to resolve the low-velocity components of the lines, therefore do not represent the true wind velocity of the unshocked CSM.

From the size of the remnant, Smith et al. ([2007](#)) estimated an upper limit of free-expansion velocity of ~4000 km s^{-1}. If the expansion velocity remained constant, in the age of 36 yr this remnant would further expand into ~0.3 pc diameter, which is still much too small to be resolved with the IFU data at hand. New VLBI observations at 8.4 GHz has been obtained in 2015 by Ryder et al. (private communication). Their data suggest that after 37 yr the remnant is still barely resolved with a diameter of <5 mas (<0.1 pc), implying that the past average expansion velocity is actually ≲1500 km s^{-1}. This is the upper limit of the past average expansion velocity and the actual current value would be smaller, though the exact value is unknown. Since the expansion velocity of ≲1500 km s^{-1} is a 37 yr average including both pre- and post-CSM crash velocities, this would imply a pre-crash free-expansion velocity of greater than 1500 km s^{-1}.

The picture of SN 1978K would be a SN ejecta freely expanding (>1500 km s^{-1}) and crashing into an inhomogeneous CSM of dense wind (~100 km s^{-1}) that was previously ejected by the progenitor star, and greatly decelerated resulting in shocks and emissions across the electromagnetic spectrum in the X-ray, optical, and radio wavelengths. As the CSM is inhomogeneously distributed, likely in clumps or in a ring or a combination of both, some part of the ejecta continues to travel unimpeded at up to ~1500 km s^{-1} as high-velocity fragments, while the bulk of the ejecta expands at a somewhat lower velocity. The presence of low-velocity hydrogen and oxygen may indicate the mixing of hydrogen and oxygen from the high velocity to low velocity due to Rayleigh–Taylor instability.

As time proceeds, the Hα luminosity decreases due to the progressively smaller mass encountered by the ejecta. On the other hand, the Hβ/Hα ratio decreases due to the shocked region becoming progressively of higher density, which argues against the $\rho \propto r^{-2}$ CSM and probably indicating a clumpy CSM. The 500 km s^{-1} velocity displayed by the optical emission lines represents the velocity of the decelerated forward shock or the reverse shock. Another possibility is that the CSM is approximately spherical, where the ≲1500 km s^{-1} upper velocity limit derived from the radio represents the forward shock and 500 km s^{-1} represents the reverse shock. Nevertheless, in this situation typically the two velocities are similar, as long as the reverse shock is still in the outer steep density profile of the envelope. SN 1978K is well evolved, therefore it could be possible that the reverse shock already reached deep into the region in the ejecta where the density structure can be flat. In this case, it could be possible to have a large velocity difference between the forward and reverse shocks. However, as has been discussed above the evolution of the line ratios and the velocity profiles indicate that a spherically symmetric CSM is not plausible.

The mass-loss rate of the progenitor star can be estimated from the luminosity of the Hα line, as the shock in the CSM is the dominant source of luminosity (Salamanca et al. [1998](#)):

$$L_{\text{H}\alpha} = \frac{1}{4}\epsilon_{\text{H}\alpha}\frac{\dot{M}}{v_w}v_s^3. \tag{1}$$

Here, if we adopt wind velocity $v_w = 70$–100 km s^{-1} and shock velocity $v_s = 500$–600 km s^{-1}, the mass-loss rate $\dot{M}$ would be of the order of 0.01 M$_\odot$ yr^{-1}. This assumes an efficiency factor $\epsilon_{\text{H}\alpha} = 0.1$, which is actually applicable for young SNe and decreases to nearly zero with time. In the case of SN 1978K at the age of several decades, $\epsilon_{\text{H}\alpha}$ would be significantly smaller than 0.1, therefore the derived mass-loss rate of ~0.01 M$_\odot$ yr^{-1} would be a lower limit. This implies that the progenitor of SN 1978K suffered heavy mass-loss, with rate at least comparable to Type-IIn SN progenitors with the highest mass-loss rates (Kiewe et al. [2012](#)) and the averaged mass-loss rate in the events of LBV giant eruptions (Smith [2014](#)). The comparison between the observed Hα luminosity and the prediction from Chevalier & Fransson ([1994](#)) in Fig. [3](#) show that the observed Hα luminosity is about two orders of magnitude higher than the model. To first approximation, the model scales with $\dot{M}/v_w$, which assumes $\dot{M} = 50 \times 10^{-5}$ M$_\odot$ yr^{-1} and $v_w = 100$ km s^{-1}. Scaling this by two orders of magnitude would require a mass-loss rate of the order of ~0.05 M$_\odot$ yr^{-1} for similar wind velocities, which is quite consistent with the value calculated above.

The CSM density parameter A_* is defined as proportional to $\dot{M}/v_w$, assuming a steady-state mass-loss, where $A_* = 100$ for the case of $\dot{M} = 10^{-5}$ M$_\odot$ yr^{-1} and $v_w = 10$ km s^{-1} (Maeda [2012](#)). For SN 1978K, adopting the wind velocity and mass-loss rate derived above, this would result in an extremely high-density CSM with $A_* \sim 1.4 \times 10^4$. This is several orders of magnitude higher than the derived values for evolved massive stars such as Wolf–Rayet and red/yellow supergiant stars, and some well-studied Type-IIb SN progenitors (Maeda et al. [2015](#)).

Following equation 2 of Patat, Chugai & Mazzali ([1995](#)), we estimate the amount of ionized hydrogen in the CSM of SN 1978K using the Hα line luminosity. This equation essentially calculates the number of recombinations of ionized hydrogen that gives rise to the Hα emission, and does not strongly depend on the CSM geometry. Assuming model A velocity structure, the amount of ionized hydrogen at the age of 36 yr would be ~0.7 M$_\odot$ if electron density is equal to proton density ($n_e = n_{\text{H}^+}$). By comparing the relative flux $L_{\text{H}\alpha}/L_{\text{He I}} \propto 1.3n_{\text{H}^+}/n_{\text{He}^+}$ (Case B recombination; Osterbrock & Ferland [2006](#)), it is found that $n_{\text{H}^+}/n_{\text{He}^+} = 5.9$. This would mean that the CSM is composed of ~86 per cent of H+ and ~14 per cent of He+. Thus, the electron density n_e would correspond to $100/86 \approx 1.2n_{\text{H}^+}$. Adopting this value of electron density would increase the estimated H envelope mass by a factor of $\sqrt{1.2}$, and therefore would not significantly change the derived value of $M_{\text{H}^+} \sim 0.7$ M$_\odot$.

Electron density can be estimated using line ratios from specific ions that were emitted by different levels with similar excitation energy, such as [S II] $\lambda6716/\lambda6731$ (Osterbrock & Ferland [2006](#)). The observed line ratio in SN 1978K is close to 0.2, which corresponds to high electron density exceeding 10^5 cm^{-3}. Chu et al. ([1999](#)) estimated the electron density to be $(3$–$12) \times 10^5$ cm^{-3}. Using equation 4 of Salamanca et al. ([1998](#)), the radius of the shock is estimated to be ~0.05–0.10 pc if electron density is between 12 and 3×10^5 cm^{-3}. The explosion energy was then estimated by

making use of equation 2.8 of Chevalier & Fransson (1994). The equation calculates the shock radius from the mass-loss rate, wind velocity, SN age, and reference density of the stellar density profile ρ_r. Assuming a flat outer density profile ($n = 7$), ρ_r was estimated to be 0.05×10^{-16} g cm^{-3} if the shock radius was 0.05 pc. A larger shock radius of 0.10 pc yields $\rho_r = 1.69 \times 10^{-16}$ g cm^{-3}. Table 1 of Chevalier & Fransson (1994) gives the values of ρ_r for set explosion energy of $E = 10^{51}$ erg and ejecta mass of $M = 10$ M$_\odot$. As the density scales with E^2/M ($n = 7$), the ρ_r values are used to scale and estimate the explosion energy of SN 1978K to be in the range of $\sim$0.1–2.0×10^{51} erg, assuming an ejecta mass of 10 M$_\odot$.

Looking back at the historic light curve presented in Fig. 1, the sudden brightening in the mid-1980s is strikingly apparent. If this sudden brightening is interpreted as the result of the interaction between the SN ejecta and the CSM, the CSM would be located at less than 0.01 pc away assuming an ejecta expanding at 1500 km s^{-1}. CSM located at this distance would require it to be produced by the dense progenitor wind $\sim$150 yr before the explosion. As the average pre-shock expansion velocity is likely to be higher than 1500 km s^{-1}, the actual distance to the CSM would be larger thus it should have been formed earlier. The interaction-powered luminosity evolution approximately follows a power-law decay, represented with a dashed line in Fig. 1. Bumps above the line (data points around 1990 and 1996) may indicate that the CSM is clumpy, causing temporary brightness increases when the shock lights up the clumps.

By assuming the volume of the CSM, the total mass of hydrogen in the CSM can be estimated by multiplying it with the hydrogen number density and the mass of a hydrogen atom. With a number density of 10^5 cm^{-3} and assuming a spherically distributed CSM with an upper limit of radius of 0.05 pc as constrained by the 2015 VLBI observations, this will amount to about 1.3 M$_\odot$ of hydrogen in the CSM. However, as previously discussed the CSM geometry is likely to be non-spherical, and its size smaller and would not fully fill the sphere with 0.05 pc radius. Furthermore, the clumpy or ring-like CSM would not subtend a solid angle encompassing the entire surface of the shell therefore the actual CSM mass should not exceed 1.3 M$_\odot$. Note that the amount of ionized hydrogen derived using the Hα line luminosity is about 0.7 M$_\odot$, in agreement with this estimate. While R93 proposed a high CSM mass of >80 M$_\odot$ in a large ($\sim$0.1 pc) CSM shell, C95 proposed a clumpy model of CSM to derive the mass of $\sim$1 M$_\odot$. Our estimates are more consistent with a $\lesssim$1 M$_\odot$ CSM, and concur with the picture proposed by Chu et al. (1999) where the SN ejecta is significantly decelerated by a dense, closer CSM although the exact geometry of the CSM is unknown.

4.2 Luminosities and comparison with other SNe

The evolution of SN 1978K during the 1980s has been investigated by R93. After the 1978 event, the object faded to its pre-SN magnitude and remained so from at least 1981, then slowly brightened again towards the end of the decade. The 843 MHz radio light curve shows that it peaked around the year 1984 (R93), while in the 5 GHz band the peak occurred in early 1981 (S99). Far-infrared *IRAS* data shows that the SN was not detected in 1983, corresponding to an upper limit of 5×10^{40} erg s^{-1} at 10 µm. Tanaka et al. (2012) suggested the presence of shocked 1.3×10^{-3} M$_\odot$ of circumstellar silicate dust in SN 1978K from the analysis of the infrared SED from 2006 to 2007 *AKARI* and *Spitzer* data. The derived infrared luminosity was 1.5×10^{39} erg s^{-1}.

X-ray observations in 1980 with the *Einstein* X-ray satellite did not detect the SN down to an unabsorbed luminosity 2.0×10^{39} erg s^{-1}, while the 1991 *ROSAT* observation showed that SN 1978K had brightened to 9.5×10^{39} erg s^{-1} in the 0.2–2.4 keV range. The most recent result by Smith et al. (2007) showed that the X-ray unabsorbed luminosity within 0.2–10 keV is 2.9×10^{39} erg s^{-1}. Dwarkadas (2014) showed that X-ray luminosities of core-collapse SNe are typically lower than 10^{39} erg s^{-1} after $\sim$10^4 d, with SNe IIn exhibiting the highest luminosity compared to the other SN subclasses. This is comparable with the exceptionally high X-ray luminosity of SN 1978K, even decades after the explosion. Thermal X-ray emission flux increases with the square of wind density, thus the interpretation is consistent with SN 1978K having exploded into a circumstellar environment dominated by a dense wind typical of SNe IIn. The fact that SN 1978K did not show strong radio and X-ray emissions during the earliest years suggests that the immediate CSM could have been sparse.[8] This is probably analogous to SN 1996cr, which was suspected to explode in a cavity-like environment before eventually the ejecta strikes a dense surrounding CSM (Bauer et al. 2008). The CSM around SNe nevertheless exhibit various structures. The Type-II SN 1996al, for example, has recently been shown to interact with a complex CSM, consisting of a dense inner CSM and equatorial ring embedded in a less dense but clumpy halo (Benetti et al. 2016).

Fig. 8 shows the comparison of the late-time spectrum of SN 1978K to those of several Type-II SNe. The spectrum of SN 2009ip[9] was obtained in 2014 in the same observing programme as SN 1978K, using the identical VLT/VIMOS instrument setup. Spectra of SNe 1995G, 1988Z, and 2004et were obtained from the SUSPECT[10] Online Supernova Spectrum Archive, while SN 1993J was from the WISeREP[11] repository (Yaron & Gal-Yam 2012). From the figure it is apparent that the current spectrum of SN 1978K does not resemble SNe IIb and IIP during their first decade. It bears more similarities with some SNe IIn, although there are also notable differences. All of the spectra exhibit dominant Balmer lines, and also the indication of iron lines around $\sim$5200–5400 Å. He I lines at λ5876 and λ7065 are also present in the SNe IIn. The dominant, narrow [N II] λ5755, He I λ5876 and [O I] $\lambda\lambda$6300, 6364 are seen in SN 1978K.

The location of SN 1978K in the host galaxy is also somewhat consistent with Type-IIn SNe on average. It is located in the host outskirts, nearly 6 kpc from the galaxy centre and in the immediate surroundings of SN 1978K there is no star formation detected. This is similar to SN 2009ip which also exploded in the outskirts of its host galaxy, in a region with insignificant star formation. Habergham et al. (2014) showed that Type-IIn SNe are weakly associated with ongoing star formation, a puzzling fact since these SNe are often associated with massive LBV stars. Smith & Tombleson (2015) noticed the isolated nature of LBV stars in the Milky Way and Magellanic Clouds, and suggested that they are mass gainers that

---

[8] The *Einstein* satellite could have detected SN 1978K were it brighter, while at that time an interferometer like *ATCA* was not yet available in order to resolve the SN flux from the host galaxy even if it was above the detection limit. The model light curve fits in fig. 10 of S99 indicate a peak flux in the decade following the explosion of close to 1 Jy, which would have easily been detectable with e.g. the Parkes radio telescope were it well resolved.

[9] We note that the nature of SN 2009ip as a genuine SN explosion is still unclear (see e.g. Margutti et al. 2014; Fraser et al. 2015). The age of 2 yr in Fig. 8 is with reference to the 2012 event.

[10] http://www.nhn.ou.edu/~suspect/

[11] http://wiserep.weizmann.ac.il/
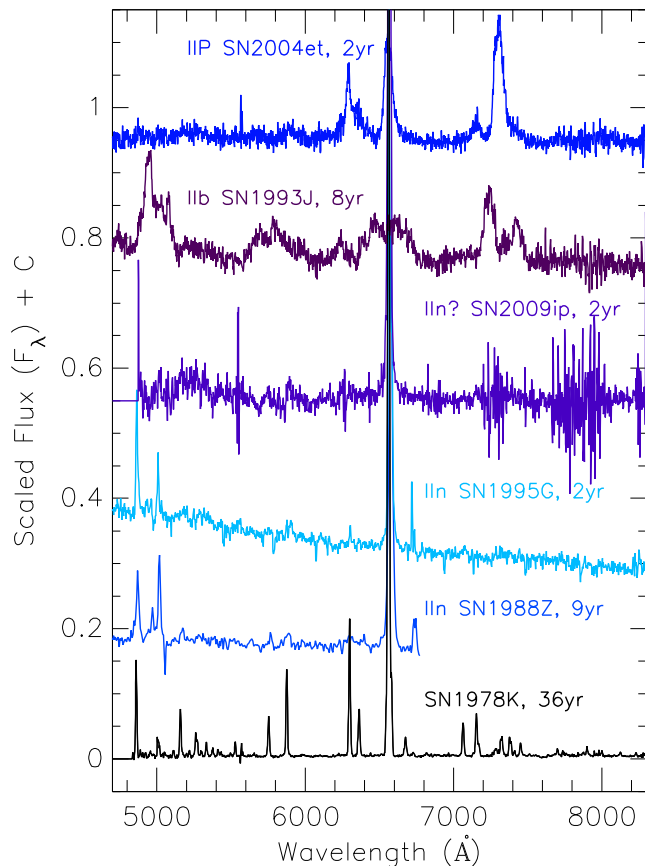
Figure 8. Comparison of 2014 SN 1978K spectrum with several Type-II SNe observed at late times. The spectrum of SN 1995G is published in Pastorello et al. (2002), SN 1988Z in Aretxaga et al. (1999), SN 1993J in Modjaz et al. (2014), and SN 2004et in Sahu et al. (2006).

were kicked out of binary systems following the SN explosion of the mass donor companion. Note that in general Type-II SNe do not follow closely the ongoing star formation as traced by H II regions (Anderson et al. 2012; Galbany et al. 2014).

4.3 Comparison with SN 1987a

It is interesting to compare the spectrum of SN 1978K with the nearest modern supernova, SN 1987A. Fig. 9 shows the comparison of SN 1978K at 2014 (age 36 yr) with SN 1987A at 1990 and 2013 (age 3 and 26 yr, respectively). We obtained the 1990 spectrum of SN 1987A (Pun et al. 1995) from SUSPECT, while the 2013 VLT/UVES echelle spectrum was taken from the ESO Science Archive Facility, Phase 3 data release of observing programme 092.D-0119 (Fransson et al. 2013, 2015). SN 1987A, due to its proximity, is spatially resolved and has been very well monitored up until very late phase where the SN ejecta interact with the distinct ring-shaped CSM. The emergence of hot spots in the ring indicates the interaction between the blast wave (forward shock) and the CSM ring, which occurred first in 1995, or 8 yr after the SN explosion (Lawrence et al. 2000). The interaction greatly decelerates the SN ejecta and generates reverse shock in the inner radius of the ring (Sonneborn et al. 1998).

The comparison between SN 1978K and SN 1987A in Fig. 9 immediately shows that the spectra of the two objects at the age of ∼3 decades look very similar. Nearly the same set of emission lines appear in both SNe, with similar relative strengths. This suggests that the SNe are in the same phase of evolution to become young SN remnants, and that similar physical processes are taking place. In SN 1987A, we detect the [Fe XIV] λ5303 line and there is no indication of [Fe X] λ6374 as is the case for SN 1978K (cf. Section 3.2). As exemplified by SN 1987A where the initially broad spectral lines evolve to become much narrower, this indicates that indeed there is a presence of dense CSM around SN 1978K that is decelerating the expansion of the ejecta ($\sim 10^3$–10^4 km s^{-1} assuming typical SN ejecta velocities; initially ∼35 000 km s^{-1} in the case of SN 1987A) thus creating shocks and slowly declining post-interaction light curve (see Fig. 1). The striking similarity of the late-time light curves of SN 1978K and 1987A again suggests the similar processes of interaction in the two SNe although the time of the onsets may be different. The peak of SN 1987A interaction light curve occurred around day 8000 (Fransson et al. 2015), or 22 yr after the SN, while in SN 1978K it occurred after ∼12 yr, indicating a relatively closer CSM concentration. This could further imply that the progenitor of SN 1978K changed its mass-loss rate in a shorter time-scale prior to the explosion compared to what SN 1987A progenitor did, assuming similar ejecta velocities and progenitor wind speeds.

In SN 1987A the shock propagates at ∼540 km s^{-1} through the unshocked (∼10 km s^{-1}) circumstellar ring and accelerates the post-shock gas (Fransson et al. 2015), resulting in typical line velocities of ∼300 km s^{-1} (Gröningsson et al. 2008) in the shocked hot spots. In this regard, one may even speculate that the CSM geometry in SN 1978K resembles the ring structure and the SN might be regarded as a more distant version of the SN 1987A remnant. R93 suggested that the peak magnitude of SN 1978K as a Type-IIP or IIL SN could have reached $M_B \sim -14$ to -15 mag, with the caveat that the 1978 light curve is very poorly sampled, thus it could have been a subluminous or even a non-terminal explosion. Note that SN 1987A, now considered a peculiar Type-II SN, is also somewhat underluminous with peak $M_V \approx -16$ mag (Schaeffer et al. 1987).

The emission of radiation from the SN 1987A ring is now decaying as the interaction proceeds to destroy it (Fransson et al. 2015). The same process is possibly also happening in SN 1978K as the late-time light curve suggests. This corroborates the fact that the spectrum has changed very little in the last 20 yr. Observations of this object in the following years/decades may reveal the weakening and eventual disappearance of the emissions from the CSM interaction. It would undoubtedly be interesting to resolve the remnant and CSM of SN 1978K and compare it to SN 1987A, although such observational effort would only be possible to be achieved using interferometry or the next generation 30 m-class telescopes operating at diffraction limit in the infrared.

5 SUMMARY

We present late-time optical spectroscopy of SN 1978K in NGC 1313, obtained in 2007 and 2014.[12] The spectrum still exhibits strong narrow emission lines (FWHM ≲600 km s^{-1}) and has not changed much since the last published observations in the 1990s. We derive a progenitor mass-loss rate of greater than 0.01 M$_\odot$ yr^{-1} and CSM mass of less than ∼1 M$_\odot$. Emission line ratios suggest that the CSM is more likely to be inhomogeneous, and the increasingly metal-rich inner ejecta is progressing to overtake the reverse shock.

---

[12] Spectra available at the WISeREP data base.
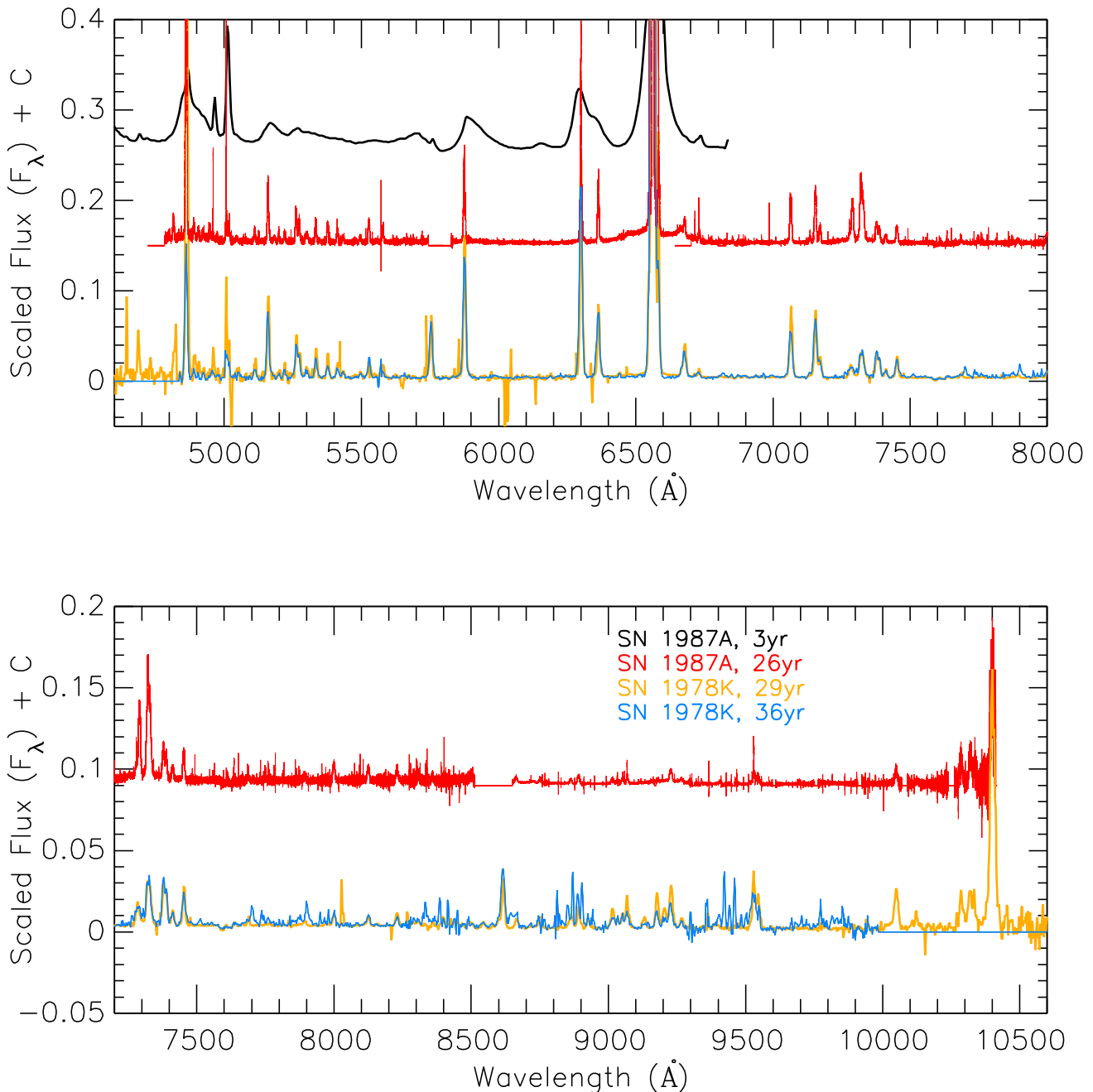
Figure 9. Comparison of SN 1978K spectrum with SN 1987A observed at late times. The nebular spectrum of SN 1987A was initially showing broad emission lines, which eventually becomes narrow similar to what is now observed on SN 1978K. The SN 1987A spectra includes the central ejecta and the CSM ring regions inside the slit (see Fransson et al. 2013).

The late-time light curve suggests that the interaction between SN blastwave and the CSM started around early to mid-1980s, and is currently decaying slowly. This behaviour is akin to SN 1987A, and the SN 1978K spectra are strikingly similar to that of SN 1987A at 26 yr. We infer that SN 1978K is currently undergoing analogous process as SN 1987A in a similarly inhomogemeous circumstellar environment where CSM interaction decays as the SN proceeds to evolve into a remnant. Continuous monitoring of this interesting object in the coming years in all accessible wavelengths is strongly encouraged.

REFERENCES

Anderson J. P., Habergham S. M., James P. A., Hamuy M., 2012, MNRAS, 424, 1372

Appenzeller I. et al., 1998, The Messenger, 94, 1

Aretxaga I., Benetti S., Terlevich R. J., Fabian A. C., Cappellaro E., Turatto M., della Valle M., 1999, MNRAS, 309, 343

Bartel N., Bietenholz M. F., Rupen M. P., Dwarkadas V. V., 2007, ApJ, 668, 924

Bauer F. E., Dwarkadas V. V., Brandt W. N., Immler S., Smartt S., Bartel N., Bietenholz M. F., 2008, ApJ, 688, 1210

Benetti S. et al., 2016, MNRAS, 456, 3296

Cardelli J. A., Clayton G. C., Mathis J. S., 1989, ApJ, 345, 245

Chevalier R. A., Fransson C., 1994, ApJ, 420, 268

Chu Y.-H., Caulet A., Montes M. J., Panagia N., Van Dyk S. D., Weiler K. W., 1999, ApJ, 512, L51

Chugai N. N., Danziger I. J., della Valle M., 1995, MNRAS, 276, 530 (C95)

Crowther P. A., 2013, MNRAS, 428, 1927

Dopita M. A., Ryder S. D., 1990, IAU Circ., 4950, 3

Dwarkadas V. V., 2014, MNRAS, 440, 1917

Fransson C. et al., 2013, ApJ, 768, 88

Fransson C. et al., 2015, ApJ, 806, L19

Fraser M. et al., 2015, MNRAS, 453, 3886

Freudling W., Romaniello M., Bramich D. M., Ballester P., Forchi V., García-Dabló C. E., Moehler S., Neeser M. J., 2013, A&A, 559, A96

Gal-Yam A., Leonard D. C., 2009, Nature, 458, 865

Galbany L. et al., 2014, A&A, 572, A38

Gröningsson P. et al., 2008, A&A, 479, 761

Gruendl R. A., Chu Y.-H., Van Dyk S. D., Stockdale C. J., 2002, AJ, 123, 2847

Habergham S. M., Anderson J. P., James P. A., Lyman J. D., 2014, MNRAS, 441, 2230

Kankare E. et al., 2012, MNRAS, 424, 855

Kiewe M. et al., 2012, ApJ, 744, 10

Kuncarayakti H. et al., 2015, Publication of Korean Astronomical Society, 30, 139

Landolt A. U., 2009, AJ, 137, 4186

Lawrence S. S., Sugerman B. E., Bouchet P., Crotts A. P. S., Uglesich R., Heathcote S., 2000, ApJ, 537, L123

Le Fèvre O. et al., 2003, Proc. SPIE, 4841, 1670

Leibundgut B., Kirshner R. P., Pinto P. A., Rupen M. P., Smith R. C., Gunn J. E., Schneider D. P., 1991, ApJ, 372, 531

Lenz E., Schlegel E. M., 2007, AJ, 134, 1821

Maeda K., 2012, ApJ, 758, 81

Maeda K. et al., 2015, ApJ, 807, 35

Margutti R. et al., 2014, ApJ, 780, 21

Mauerhan J., Smith N., 2012, MNRAS, 424, 2659

Milisavljevic D., Fesen R. A., Leibundgut B., Kirshner R. P., 2008, ApJ, 684, 1170

Milisavljevic D., Fesen R. A., Kirshner R. P., Challis P., 2009, ApJ, 692, 839

Milisavljevic D., Fesen R. A., Chevalier R. A., Kirshner R. P., Challis P., Turatto M., 2012, ApJ, 751, 25

Modjaz M. et al., 2014, AJ, 147, 99

Osterbrock D. E., Ferland G. J., 2006, Astrophysics of Gaseous Nebulae and Active Galactic Nuclei, 2nd edn. University Science Books, Mill Valley, CA

Ott T., 2012, Astrophysics Source Code Library, 1210.019

Pastorello A. et al., 2002, MNRAS, 333, 27

Patat F., Chugai N., Mazzali P. A., 1995, A&A, 299, 715

Pun C. S. J. et al., 1995, ApJS, 99, 223

Qing G., Wang W., Liu J.-F., Yoachim P., 2015, ApJ, 799, 19

Ryder S., Staveley-Smith L., Dopita M., Petre R., Colbert E., Malin D., Schlegel E., 1993, ApJ, 416, 167 (R93)

Ryder S. D., Staveley-Smith L., Malin D., Walsh W., 1995, AJ, 109, 1592

Sahu D. K., Anupama G. C., Srividya S., Muneer S., 2006, MNRAS, 372, 1315

Salamanca I., Cid-Fernandes R., Tenorio-Tagle G., Telles E., Terlevich R. J., Munoz-Tunon C., 1998, MNRAS, 300, L17

Schaeffer R., Casse M., Cahen S., Mochkovitch R., 1987, A&A, 184, L1

Schlegel E. M., Ryder S., Staveley-Smith L., Petre R., Colbert E., Dopita M., Campbell-Wilson D., 1999, AJ, 118, 2689 (S99)

Silva-Villa E., Larsen S. S., 2012, MNRAS, 423, 213

Smith N., 2014, ARA&A, 52, 487

Smith N., Tombleson R., 2015, MNRAS, 447, 598

Smith I. A., Ryder S. D., Böttcher M., Tingay S. J., Stacy A., Pakull M., Liang E. P., 2007, ApJ, 669, 1130

Smith N. et al., 2011, ApJ, 732, 63

Sonneborn G. et al., 1998, ApJ, 492, L139

Taddia F. et al., 2013, A&A, 555, A10

Tanaka M. et al., 2012, ApJ, 749, 173

Yaron O., Gal-Yam A., 2012, PASP, 124, 668

This paper has been typeset from a TEX/LATEX file prepared by the author.